TABLE I

Z mm	0	0.002	0.004	0.005	0.01	0.02	0.03	0.04	0.05	0.1	0.5	1	1.5	2	3
Real $\sigma(z)$ $(ohm.m)^{-1}$	33	26	16	10	6	2.3	1.25	0.75	0.5	0.2	0.2	0.2	0.2	0.2	0.2
Initial $\sigma(z)$ $(ohm.m)^{-1}$	35	32	30	27	22	13	8	4.75	4	0.4	0.4	0.4	0.4	0.4	0.4
Reached $\sigma_1(z)$ $(ohm.m)^{-1}$	33.2	26.2	16.5	11	6.5	2.5	1.25	0.75	0.5	0.25	0.22	0.21	0.22	0.22	0.22

realized after one cycle. For the real pulsating $\epsilon_b'(z)$ a solution $S_b(z)$ is reached after four iterations.

Example 3

Table I illustrates the application of the gradient technique for obtaining the conductivity profile of a lossy semiconductor which has $\epsilon'(z) = 12 - Z/L$ and unknown inhomogeneous $\sigma(z)$. The layer thickness is 3 mm, $N = 16$, and the frequency is 10 GHz. From the table it is clear that the obtained $\sigma_1(z)$ distribution is very close to the real one. The only limitation, on solving for semiconductors having high parameter values, is to optimize the layer thickness by

$$\bar{\lambda}/4 < L < \bar{\lambda}/2$$

where $\bar{\lambda}$ is the average wavelength in the tested sample. This limitation ensures that variations in the measured reflection coefficients are due to load variations.

VI. Discussion and Conclusions

It is clear from the above numerical experiments that the iterative technique of the FGM is very efficient in determining the inhomogeneous profile of the complex dielectric constant of materials. The functional reaches its global minimum in a finite number of iterative cycles and the final solution obtained is unique and independent of the initial guess. One need not have *a priori* information about the medium, but only information about the maximum and minimum values of the desired function. The FGM does not have restrictions on the initial solution and it is applicable with good approximations to discontinuous functions. The number of measurements N must be sufficient to give true information about the probed medium, and optimum N is given by $20 > N > 12$. All the N measurements are carried out at a single frequency. The frequency error (Δf) must not exceed 5 percent. At 36.524 GHz (for a medium which has an average $\epsilon'(z) = 12$ and $\sigma(z) = 5$), $\Delta f = \pm 6$ percent will cause errors in the evaluated reflection coefficients; $\Delta R = \pm 3.5$ percent and $\Delta Q = \pm 8.477$ percent. The corresponding errors in the reconstructed $\epsilon'(z)$ and $\sigma(z)$ are ± 4.55 percent and ± 8.3 percent, respectively. These error values will differ for different materials.

References

[1] A. V. Tikhonravov, "Synthesis problem of stratified medium having a function distribution of parameters," *Sov. Opt. Spectroscopy*, vol 24, no. 6, pp. 1185–190, 1977.

[2] T. K Sarkar, E. Arvas, and S. M Reo, "Application of FFT and the conjugate gradient method for the solution of electromagnetic radiation from electrically large and small conducting bodies," *IEEE Trans. Antennas Propagat*, vol. AP-34, pp. 635–640, May 1986

[3] V. A. Morozov, *Methods for Solving Incorrectly Posed Problems*. New York: Springer-Verlag, 1984.

[4] A. N. Tikhonov and V. U. Arcenin, *Methods of Solving Incorrect Problems* Moscow: Nauka, 1979.

[5] J. C. Bolomey, D. Lesselier, C. Pichot, and W. Tabbara, "Spectral and time domain approaches to some inverse scattering problems," *IEEE Trans. Antennas Propagat.*, vol. AP-29, pp. 206–212, Mar. 1981

[6] S. Coen, "Inverse scattering of a layered and dispersionless dielectric half-space, Part 1: Reflection data from plane wave at normal incidence," *IEEE Trans Antennas Propagat*, vol. AP-29, pp. 726–732, Sept 1981.

[7] A. G. Tijhuis and C Van Der Worm, "Iterative approach to the frequency-domain solution of the inverse-scattering problem for an inhomogeneous lossless dielectric slab," *IEEE Trans. Antennas Propagat.*, vol AP-32, pp. 711–716, July 1984.

[8] M A. Hindy, "Gradient method for the solution of microwave inverse problems of semiconductors," presented at 29th Midwest Symp. Circuits Syst., 1986.

Transmission Properties of a Right-Angle Microstrip Bend with and Without a Miter

ANTONIOS D. BROUMAS, HAO LING, MEMBER, IEEE, AND TATSUO ITOH, FELLOW, IEEE

Abstract **— Based on the waveguide model, the transmission properties of a microstrip bend with and without a miter are investigated using the Green's theorem approach. Unlike the conventional mode-matching technique, this approach does not require a modal description of fields inside the discontinuity region. Scattering parameters for the bend are presented. They agree well with the quasi-static results at low frequencies. Significant improvement in the transmission properties is observed for the bend with a miter.**

I. Introduction

A right-angle microstrip bend is one of the most common discontinuities encountered in microstrip-based integrated circuits. It is normally used to provide flexibility in circuit layout. Accurate characterization of the transmission properties of a microstrip bend therefore plays an important role in the success-

Manuscript received June 6, 1988; revised November 21, 1988 This work was supported by the National Science Foundation under Grant ECS-8657524 and by the Army Research Office under Contract DAAL 03-88-K-0005.

The authors are with the Department of Electrical and Computer Engineering, University of Texas at Austin, Austin, TX 78712

IEEE Log Number 8926578.

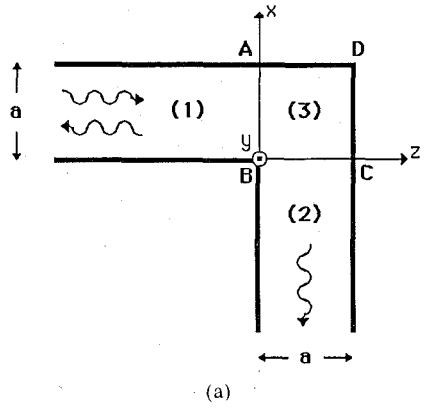

(a)

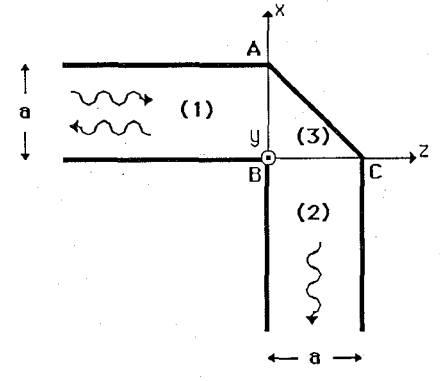

(b)

Fig. 1. Top view of the right-angle microstrip bend. (a) Without miter. (b) With miter.

ful implementation of computer-aided design tools, especially in the higher frequency regimes.

The microstrip waveguide model has been applied extensively to various microstrip discontinuities such as T junctions, crossings, and steps [1]–[3]. In terms of the frequency range of applicability, the waveguide model provides an "intermediate" solution which surpasses the accuracy of the quasi-static analysis and provides accurate magnitude information on the scattering parameters. In this paper, a right-angle microstrip bend is characterized based on the waveguide model. In addition, the effect of a 45° miter at the outer portion of the right-angle bend is investigated. The geometries of the bend without a miter and the bend with a miter are shown in Figs. 1(a) and (b), respectively.

Our approach to the microstrip bend problem will not be the conventional mode-matching technique discussed in detail in [1]–[5]. Instead, a Green's theorem approach first suggested by Whitehead [6] and later utilized by Itoh and Mittra [7] in the analysis of grating structures will be applied to the waveguide discontinuity problem at hand. The premise of this approach is based on the observation that often the actual fields inside the discontinuity region are of no interest to us. Therefore, it is highly undesirable having to first determine the complicated modal description of the fields in the discontinuity region, such as region (3) in Fig. 1(b). The technique we will adopt is based on an elegant application of the Green's theorem [8] which allows us to relate modes on the two sides of the discontinuity without actually calculating the fields inside the discontinuity region. By properly choosing a set of auxiliary functions which satisfy the source-free wave equation, a matrix equation similar to that resulting from the mode-matching technique can be obtained.

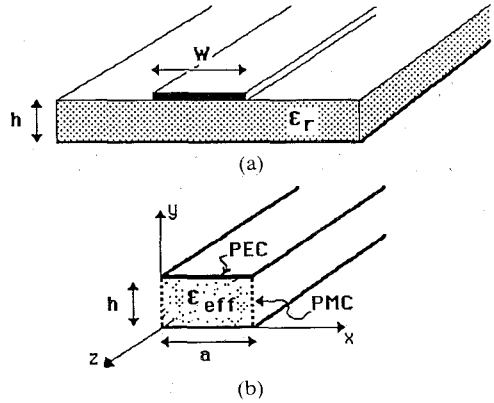

(a)

(b)

Fig. 2. Waveguide model for the microstrip line.

II. Formulation

Referring to Fig. 2(a), the microstrip line is modeled as a waveguide with perfect magnetic conducting (PMC) sidewalls as shown in Fig. 2(b). The thickness of the dielectric (h) should be less than the width of the strip (W). The smaller the h the more accurate the waveguide model. In order to take into account the fringe field, an effective width, a, and an effective dielectric constant, ϵ_{eff}, are introduced. For the selection of a and ϵ_{eff}, see [9]–[11].

In the waveguide of Fig. 2(b), a TEM mode can be supported. The frequency $c/2a$, where c is the speed of light in ϵ_{eff}, corresponds to the cutoff frequency of the first non-TEM mode. Since both the incidence field of interest and the geometry of the structure are independent of y, we expect that in the neighborhood of the discontinuity only modes which are independent of y will be excited. As we can see by a simple inspection of TE_{mn} and TM_{mn} modes, the only such modes are the TE_{m0} modes, $m=0,1,2,\cdots$, where TE_{00} is the TEM mode. Therefore, in region (1) the fields can be expanded as follows:

$$E_{y1}(x,z)=\left(C_0^{1+}e^{-jkz}+C_0^{1-}e^{+jkz}\right)+\sum_{m=1}^{\infty}\left(C_m^{1+}e^{-\gamma_m z}+C_m^{1-}e^{+\gamma_m z}\right)\cos\left(\frac{m\pi x}{a}\right)$$

$$H_{x1}(x,z)=\left(-C_0^{1+}e^{-jkz}+C_0^{1-}e^{+jkz}\right)\frac{\omega\epsilon}{k}+\sum_{m=1}^{\infty}\left(-C_m^{1+}e^{-\gamma_m z}+C_m^{1-}e^{+\gamma_m z}\right)\frac{\gamma_m}{j\omega\mu}\cos\left(\frac{m\pi x}{a}\right)$$

$$H_{z1}(x,z)=\sum_{m=1}^{\infty}\left(C_m^{1+}e^{-\gamma_m z}+C_m^{1-}e^{+\gamma_m z}\right)\cdot\frac{\gamma_m}{j\omega\mu a}\sin\left(\frac{m\pi x}{a}\right) \tag{1}$$

where $\gamma_m=[(m\pi/a)^2-k^2]^{1/2}$, $k=\omega/c$, and $\epsilon=\epsilon_{\text{eff}}\epsilon_0$. The square root for γ_m is to be taken as positive for both real and imaginary cases. Similarly in region (2), using a rotation of coordinates, we can write

$$E_{y2}(x,z)=C_0^{2+}e^{+jkx}+\sum_{m=1}^{\infty}C_m^{2+}e^{+\gamma_m x}\cos\left(\frac{m\pi z}{a}\right)$$

$$H_{z2}(x,z)=C_0^{2+}e^{+jkx}\frac{\omega\epsilon}{k}+\sum_{m=1}^{\infty}C_m^{2+}e^{+\gamma_m x}\frac{\gamma_m}{j\omega\mu}\cos\left(\frac{m\pi z}{a}\right)$$

$$H_{x2}(x,z)=\sum_{m=1}^{\infty}C_m^{2+}e^{+\gamma_m x}\frac{m\pi}{j\omega\mu a}\sin\left(\frac{m\pi z}{a}\right). \tag{2}$$

Note that the problem becomes in fact a two-dimensional one after the elimination of the y-dependent modes. Although the

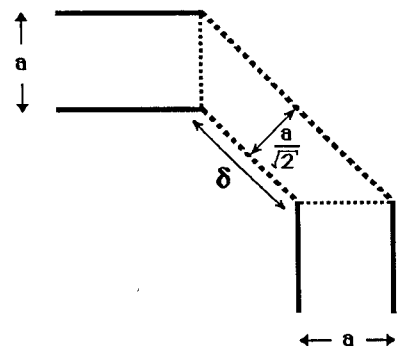

Fig. 3. Conceptual motivation for selecting the auxiliary function G in solving the microstrip bend problem with a miter.

TEM mode is of most interest, we have kept the formulation general enough to handle any combination of TE_{m0} modes as the incident excitation.

Next we observe that a unique solution for the fields in region (3) must exist. It matches with the fields in regions (1) and (2) on the surfaces $(AB \times h)$ and $(BC \times h)$ and obeys the boundary condition on the PMC walls $(CD \times h)$ and $(DA \times h)$, or $(CA \times h)$ in the case of a miter. Also it is sufficient to work with only one field component. The E_y component will be used implicitly in order to obtain a sufficient number of equations relating C_m^{1+}, C_m^{1-}, and C_m^{2+}. These equations are obtained by applying the scalar version of the Green's theorem [8] which states that

$$\int_S \left(G \frac{\partial E_y}{\partial n} - \frac{\partial G}{\partial n} E_y \right) ds = 0. \tag{3}$$

Here G and E_y are functions obeying the source-free wave equation in a region enclosed by surface S with an outward pointing normal $\hat{n}$. In our case, E_y satisfies the source-free wave equation $(\nabla^2 + k^2) E_y = 0$ in region (3). Furthermore, $\partial E_y / \partial n = 0$ on the PMC walls. Therefore, if we select an auxiliary function G such that

$$(\nabla^2 + k^2) G = 0 \quad \text{and} \quad \frac{\partial G}{\partial n} = 0 \quad \text{on the PMC walls} \tag{4}$$

equation (3) becomes

$$\int_{AB} \left(G \frac{\partial E_y}{\partial (-z)} - \frac{\partial G}{\partial (-z)} E_y \right) dx = - \int_{BC} \left(G \frac{\partial E_y}{\partial (-x)} - \frac{\partial G}{\partial (-x)} E_y \right) dz. \tag{5}$$

This equation in fact relates the coefficients C_m^{1+}, C_m^{1-}, and C_m^{2+}. Clearly we obtain only one equation by using the Green's theorem once. Therefore, by selecting a set of auxiliary functions which satisfy (4) and by applying (5) repeatedly, we obtain a sufficient number of equations to solve for C_m^{1-} and C_m^{2+}. In general there is no formal methodology for selecting a family of auxiliary functions. The special geometry of each problem has to be considered. In this regard, the auxiliary function plays a role similar to that of the testing function in the method of moments.

A. Microstrip Bend Without Miter

We select as the auxiliary functions

$$G_{p1}(x,z) = \left(e^{-\gamma_p z} + e^{+\gamma_p z} \right) \cos\left(\frac{p\pi x}{a} \right)$$
$$G_{p2}(x,z) = \left(e^{-\gamma_p x} + e^{+\gamma_p x} \right) \cos\left(\frac{p\pi z}{a} \right), \qquad p = 0,1,2,\cdots \tag{6}$$

where γ_p is given by the same formula as γ_m. (Clearly $\gamma_0 = jk$.) Applying repeatedly equation (5) using G_{p1} and G_{p2} in place of G, we obtain a sufficient number of equations to solve for C_m^{1-} and C_m^{2+}. The equations can be cast into a $(2M \times 2M)$ matrix equation where M is the number of modes to be used in each region:

$$\begin{bmatrix} [A] & [B] \\ [B] & [A] \end{bmatrix} \cdot \begin{bmatrix} [C_m^{1-}] \\ [C_m^{2+}] \end{bmatrix} = \begin{bmatrix} [RS_{p1}] \\ [RS_{p2}] \end{bmatrix} \tag{7}$$

In the above expression, $[C_m^{1}]$, $[C_m^{2+}]$, $[RS_{p1}]$, and $[RS_{p2}]$ are $(M \times 1)$ column vectors; $[A]$ and $[B]$ are $M \times M$ matrices. The elements in the matrix equation are given below:

$$A_{pm} = \begin{cases} -\gamma_p a e^{\gamma_p a} \epsilon_p, & p = m \\ 0, & p \neq m \end{cases}$$
$$B_{pm} = \cos(p\pi)(-\gamma_m) \int_0^a \left(e^{-\gamma_p z} + e^{+\gamma_p z} \right) \cos\left(\frac{m\pi z}{a} \right) dz$$
$$RS_{p1} = -\gamma_p a e^{-\gamma_p a} C_p^{1+} \epsilon_p$$
$$RS_{p2} = \cos(p\pi) \sum_{m=0}^{\infty} (-\gamma_m) \cdot \left[\int_0^a \left(e^{-\gamma_p x} + e^{+\gamma_p x} \right) \cos\left(\frac{m\pi x}{a} \right) dx \right] C_m^{1+} \tag{8}$$

where $\epsilon_k = 1$ for $k \neq 0$ and $\epsilon_k = 2$ for $k = 0$.

B. Microstrip Bend with 45° Miter Cut

The auxiliary function G in this case is selected as

$$G_{p1}(x,z) = \cos\left[\left(\frac{p\pi}{a} \right)(x+z) \right] e^{-\gamma_p(-x+z)/\sqrt{2}}$$
$$G_{p2}(x,z) = \cos\left[\left(\frac{p\pi}{a} \right)(x+z) \right] e^{+\gamma_p(-x+z)/\sqrt{2}}, \qquad p = 0,1,2,\cdots \tag{9}$$

where $\gamma_p = \sqrt{2(p\pi/a)^2 - k^2}$. Our selection is motivated by the fact that the problem in Fig. 1(b) is the limiting case of the problem in Fig. 3 as $\delta \to 0$. This choice of G leads to a matrix equation of the same form as (7). With the same notation in subsection A, we have

$$A_{pm} = \left(-\gamma_m - \frac{\gamma_p}{\sqrt{2}} \right) \int_0^a \cos\left(\frac{p\pi x}{a} \right) e^{\gamma_p x/\sqrt{2}} \cos\left(\frac{m\pi x}{a} \right) dx + \left(-\frac{p\pi}{a} \right) \int_0^a \cos\left(\frac{m\pi x}{a} \right) \sin\left(\frac{p\pi x}{a} \right) e^{\gamma_p x/\sqrt{2}} dx$$
$$B_{pm} = \left(-\gamma_m + \frac{\gamma_p}{\sqrt{2}} \right) \int_0^a \cos\left(\frac{p\pi z}{a} \right) e^{-\gamma_p z/\sqrt{2}} \cos\left(\frac{m\pi z}{a} \right) dx + \left(-\frac{p\pi}{a} \right) \int_0^a \cos\left(\frac{m\pi z}{a} \right) \sin\left(\frac{p\pi z}{a} \right) e^{-\gamma_p z/\sqrt{2}} dx$$
$$RS_{p1} = \sum_{m=0}^{M-1} C_m^{1+} \left[\left(-\gamma_m + \frac{\gamma_p}{\sqrt{2}} \right) \cdot \int_0^a \cos\left(\frac{p\pi x}{a} \right) e^{\gamma_p x/\sqrt{2}} \cos\left(\frac{m\pi x}{a} \right) dx + \frac{p\pi}{a} \int_0^a \cos\left(\frac{m\pi x}{a} \right) \sin\left(\frac{p\pi x}{a} \right) e^{\gamma_p x/\sqrt{2}} dx \right]$$
$$RS_{p2} = \sum_{m=0}^{M-1} C_m^{1+} \left[\left(-\gamma_m - \frac{\gamma_p}{\sqrt{2}} \right) \int_0^a \cos\left(\frac{p\pi x}{a} \right) e^{-\gamma_p x/\sqrt{2}} \cdot \cos\left(\frac{m\pi x}{a} \right) dx + \frac{p\pi}{a} \int_0^a \cos\left(\frac{m\pi x}{a} \right) \cdot \sin\left(\frac{p\pi x}{a} \right) e^{-\gamma_p x/\sqrt{2}} dx \right]. \tag{10}$$

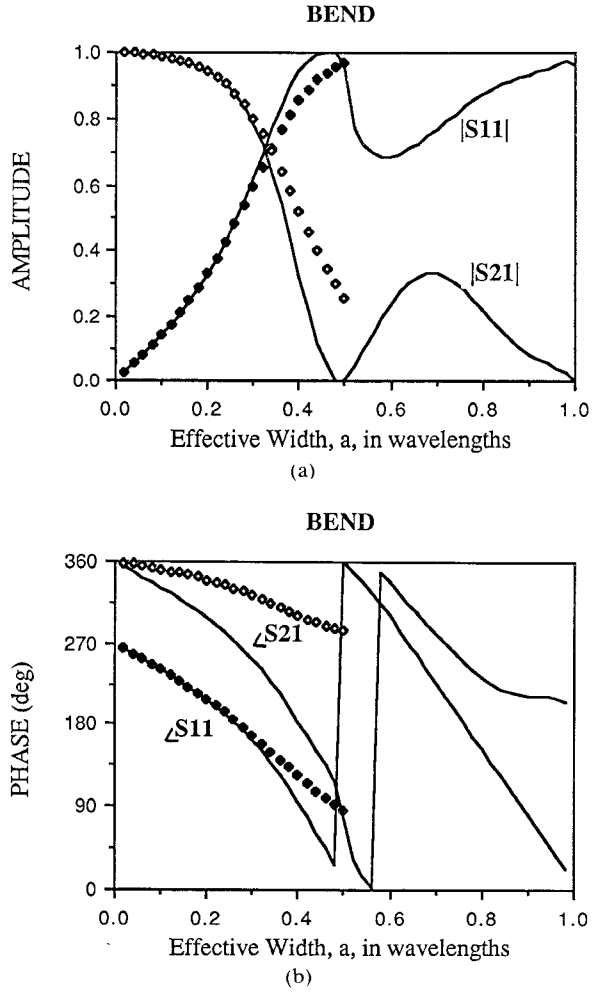

Fig. 4. Scattering parameters of a right-angle microstrip bend without miter versus the effective width of the microstrip in wavelengths. (◆ and ◇ are the quasi-static results from [12].) (a) Amplitude. (b) Phase

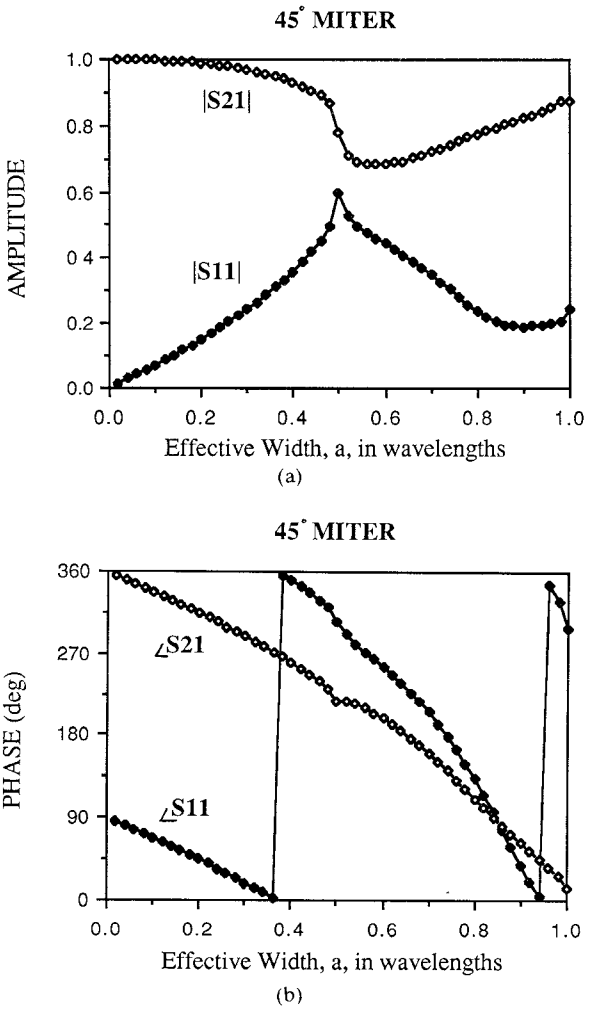

Fig. 5. Scattering parameters of a right-angle microstrip bend with a 45° miter versus the effective width of the microstrip in wavelengths. (a) Amplitude. (b) Phase.

To summarize, choices for the auxiliary functions given in (6) and (9) lead to a matrix equation of the form given in (7) for a bend with or without a miter. The scattering parameters characterizing the bend are easily obtained by solving the matrix equation.

III. Numerical Results

Shown in Fig. 4(a) are the amplitudes of the scattering parameters S_{11} and S_{21} versus the effective width in wavelengths, a/λ, for the right-angle microstrip bend without a miter. In the numerical calculation, three to four modes are satisfactory for achieving convergent results. The energy conservation criterion was checked and found to be satisfied at all frequencies up to $a/\lambda = 1$. Note that above $a/\lambda = 0.5$, both the TE_{10} and the TEM mode can propagate in the waveguide model. In the $a/\lambda < 0.5$ region, the reflection coefficient S_{11} increases monotonically as a function of frequency. Also plotted in the figure are the quasi-static results reported in [12]. As expected, the quasi-static results agree well with our data at low frequencies. Fig. 4(b) shows the phase of the scattering parameters S_{11} and S_{21}.

In Fig. 5, the amplitude and the phase of the scattering parameters for the microstrip bend with a miter are shown as functions of a/λ. For $a/\lambda < 0.5$, the numerical results again converge nicely with only three to four modes and energy conservation is satisfied. This feature does not remain valid for $a/\lambda > 0.5$. We believe this defect to be strongly related to the set of auxiliary functions we have chosen. Additional constraints such as edge conditions may need to be imposed on the auxiliary functions, in addition to those stated in (4), in order to achieve better numerical stability.

Finally, by comparing Figs. 4(a) and 5(a), we observe that the transmission properties of the bend with a miter are much superior to those of the bend without a miter. This is especially apparent at the high-frequency end.

IV. Conclusions

The Green's theorem approach has been applied to the problem of a right-angle microstrip bend with or without a miter. The microstrip waveguide model is assumed in the analysis. Unlike the mode-matching technique, this approach does not require a complete modal description of fields inside a discontinuity region. Instead, the fields on the two sides of the discontinuity are related by applying the Green's theorem with an appropriate choice of an auxiliary function which plays a role analogous to that of the testing function in the method of moments. The selection of the auxiliary function is not systematic and involves good physical insight to the problem under study.

The numerical results we have generated show that the transmission properties of the bend are significantly improved with a miter cut at the corner. By themselves, our results provide an accuracy check for the more sophisticated integral equation approach which can handle arbitrarily shaped boundaries. Moreover, with a slight modification, this technique may be extended to study microstrip corners with an arbitrary miter.

References

[1] G. Kompa and R. Mehran, "Planar waveguide model for calculating microstrip components," *Electron. Lett*, vol. 11, pp. 459–460, Sept. 1975.

[2] W. Menzel and I. Wolff, "A method for calculating the frequency-dependent properties of microstrip discontinuities," *IEEE Trans. Microwave Theory Tech.*, vol. MTT-25, pp. 107–112, Feb. 1977

[3] T. S. Chu, T Itoh, and Y.-C. Shih, "Comparative study of mode-matching formulations for microstrip discontinuity problems," *IEEE Trans. Microwave Theory Tech.*, vol. MTT-33, pp. 1018–1023, Oct. 1985.

[4] J J. Campbell and W. R. Jones, "Symmetrically truncated right angle corners in parallel plate and rectangular waveguide," *IEEE Trans. Microwave Theory Tech.*, vol. MTT-16, pp. 517–529, Aug. 1968.

[5] R. Mehran, "The frequency dependent scattering matrix of twofold truncated microstrip bends," *Arch. Elek. Übertragung.*, vol. 81, pp. 411–415, 1977.

[6] E. A. N. Whitehead, "The theory of parallel-plate media for microwave lenses," *Proc. Inst. Elec. Eng.*, vol. 98, pt. III, pp. 133–140, Jan 1951

[7] T. Itoh and R. Mittra, "An analytical study of the echelette grating with application to open resonators," *IEEE Trans. Microwave Theory Tech.*, vol. MTT-17, pp. 319–327, June 1969.

[8] R. F. Harrington, *Time-Harmonic Electromagnetic Fields*. New York: McGraw-Hill, 1961, sec. 3.4.

[9] E. Yamashita, K. Atsuki, and T. Ueda, "An approximate dispersion formula of microstrip lines for computer-aided design of microwave integrated circuits," *IEEE Trans. Microwave Theory Tech*, vol. MTT-27, pp. 1036–1038, Dec. 1979

[10] E. Hammerstad and O. Jensen, "Accurate models for microstrip computer-aided design," in *1980 IEEE MTT-S Int. Microwave Symp. Dig.*, pp. 407–409.

[11] M. Kirschning and R. H. Jansen, "Accurate wide-range design equations for the frequency-dependent characteristic of parallel coupled microstrip lines," *IEEE Trans. Microwave Theory Tech.*, vol. MTT-32, pp. 83–90, Jan. 1984.

[12] A. A. Oliner, "Equivalent circuits for discontinuities in balanced strip transmission lines," *IEEE Trans. Microwave Theory Tech.*, vol MTT-3, pp. 134–143, Nov. 1955.

The Use of a Single Source to Drive a Binary Peak Power Multiplier

P. E. LATHAM, MEMBER, IEEE

***Abstract*—The binary power multiplier (BPM) recently proposed by Farkas [1] requires a pair of RF inputs whose phases are set independently. In this note, a method is presented in which a single source may be used to drive a BPM. Phase coding occurs at the source input, where the power is low and phase switching is straightforward. There is a loss in energy of around 25 percent but only a small reduction in peak power.**

I. Introduction

Future TeV linear colliders require sources producing peak power in the 100 MW range. The exact power level depends on frequency, but present estimates are around 750 MW at 2.8 GHz [1] (SLAC frequency), 500 MW at 10 GHz [2], and 200 MW at 17 GHz [3]. When additional constraints such as high efficiency, high gain, and phase stability are introduced, these powers are beyond the state of the art of present and near-future sources. To circumvent the lack of suitable sources, pulse compression may be used to increase peak power at the expense of pulse length, thus reducing the requirements to technologically feasible levels.

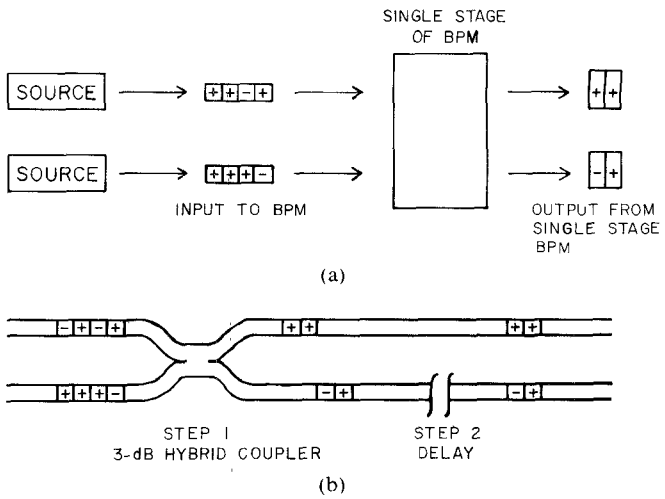

Fig 1. (a) Coding for a single-stage binary power multiplier The time bins are coded according to phase: − represents 0° and + represents 180°. On output, the pulse length is halved and the power doubled (b) Schematic of a single-stage BPM.

Recently, Farkas proposed an efficient multiple-stage pulse compression scheme [1] in which the power is doubled and the pulse length halved at each stage. The scheme is described in detail in [1]. Briefly, a single stage of the binary power multiplier (BPM) works as follows: the input into each stage consists of two pulse trains coded into time bins, with a phase of either 0° or 180° in each bin. The pulse trains are combined to produce two outputs, each at twice the power and half the duration and properly coded for the next stage. The coding for this process is illustrated schematically in Fig. 1(a), where a phase of 0° is denoted by a − and a phase of 180° by a +. The power doubling, which is shown in Fig. 1(b), occurs in two steps. First, adjacent bins are combined by a 3 dB hybrid coupler according to the rules given in [1]. Second, the leading pulse is delayed so that the bins are again adjacent. The peak power multiplication is 2^n for an n-stage device, less any losses due to nonideal properties.

This pulse compression scheme has been demonstrated at low power using both fundamental mode rectangular and TE_{01} circular waveguide [3]. While the basic validity of the binary pulse multiplication scheme was confirmed, the losses were high (greater than 40 percent power loss for the two-stage BPM). For practical applications, delay lines with acceptable wall losses and 3 dB hybrid couplers with minimal mode conversion and reflection need to be designed. In addition, problems of phase noise need to be studied, as the BPM efficiency degrades rapidly with phase jitter.

Because of the high power involved, the coding of the pair of pulses trains which enters the BPM must occur at the input end of the source, where the power is low. Consequently, two separate sources are needed to drive a single BPM if it is to operate at maximum efficiency. For testing and development, however, it is desirable to use a single source. This may be done with some decrease in energy efficiency (less than 30 percent) but little loss

Manuscript received July 27, 1988; revised November 28, 1988. This work was supported by the U.S. Department of Energy.

The author is with the Laboratory of Plasma Research, University of Maryland, College Park, MD 20742.

IEEE Log number 8926585.